Stabilization of Diamond cubic Sn Nanodots in Ge

[1]R.Goswami*, [1]S. B. Qadri, [1]E. P. Gorzkowski, [2]J. P. Yesinowski and [3]G. G. Jernigan

Abstract

Diamond cubic Sn (α-Sn) has many potential optoelectronic applications, but is normally stable only below 13ºC. Here we demonstrate the stabilization of α-Sn nanodots at room temperature and above in a Ge matrix produced by rapid solidification of a Ge-6.3 at. %Sn alloy. High resolution transmission electron microscopy (HRTEM) and differential scanning calorimetry (DSC) were employed to study the structure and stability of Sn particles, respectively. We show that the formation pathway of α-Sn is through the decomposition of a Ge-Sn solid solution, which gives a thermodynamic driving force necessary for the formation of α-Sn.

Key words: Sn Nanodots, Ge Matrix, Rapid solidification, TEM, Diamond Cubic Sn, Grey Tin

1. Introduction

The diamond cubic (dc) Sn (grey tin, or α-Sn) is the only known zero-gap 3D elemental semiconductor [1]. It has a low electron effective mass and has theoretical predictions for the opening of a bandgap in nanoscopic α-Sn due to quantum confinement effects (QCE) [2-4], suggesting potential optoelectronic applications despite bulk α-Sn being stable only below 13º C. Nanodots of α-Sn have been reported in a Si matrix and the optical properties were investigated [3, 5-6]. α-Sn nanodots were also observed in lithium ion battery anodes, where upon repeated cycling it was reported that α-Sn was more stable than the tetragonal white tin (β-Sn) with lithiation [7]. The stabilization of α-Sn in the form of thin 2D films well above room temperature was first demonstrated by molecular beam epitaxy (MBE) on lattice-matched zincblende InSb or CdTe substrate [8], and many subsequent studies have demonstrated similar behavior. The thermal stabilization may be attributed to strong bonding between α-Sn and zincblende InSb [9].

It is interesting to consider the possibility of forming α-Sn nanodots in the diamond cubic lattice of Ge, the Group IV element closest to Sn. The growth of metastable $Ge_{1-x}Sn_x$ alloys in order to create a tunable direct bandgap in a largely Ge semiconductor has been pursued by CVD [10] and MBE methods [11], both under highly nonequilibrium

conditions because of the low (<1.0 atom %) solubility of Sn in Ge and the negligibly small solubility of Ge in Sn. We report here that crystalline α-Sn nanodots ranging from 5 to 15 nm (diameter) embedded in a Ge matrix are formed by rapid solidification of a Ge-Sn alloy melt, and that these nanodots are stable to elevated temperatures.

2. Experimental:

An ingot with a nominal composition Ge-6at.%Sn was produced from elemental constituents exceeding 99.97% purity by arc melting in an inert atmosphere. A portion of the ingot was melted in an induction furnace, and subsequently the molten alloy was injected onto a rotating Cu wheel with an over pressure of 1/3 atmosphere of argon for melt spinning with a wheel speed of 25 m-s^{-1}. The resulting ribbons were characterized with a JEOL 2200 FX transmission electron microscope. To investigate the stability of Sn particles we performed differential scanning calorimetry at a scanning rate of 20°C/min.

3. Results and Discussion

Rapid solidification of Ge-6.3at.% Sn yields a dispersion of Sn particles in the Ge matrix since the Ge-Sn system has a submerged (or metastable) liquid miscibility gap because of the positive enthalpy of mixing (ΔH_{mix}) of Ge and Sn [12]. A number of coarse Sn particles with size 300 to 600 nm were observed at grain boundaries. Fig. 1 (a) is the bright-field image showing a coarse Sn particle at the triple point. All of the observed coarse Sn particles are β-Sn. On the other hand, a very fine dispersion of Sn particles with size ranging from 5 to 15 nm in diameter was observed within Ge grains (Fig. 1b). This is similar to the microstructure observed in rapidly solidified binary alloys of Al-Sn [13,14] with metastable miscibility gap. These fine Sn particles are of mixed type, the majority being α -Sn nanocrystals. Fig. (1c) shows a HRTEM-image of a fine β-Sn particle containing thick Moire fringes near to the [011] zone of Ge. The corresponding fast Fourier transform (FFT) obtained from part of the matrix and the particle is given in Fig. 1(d), showing the 200 reflection with d-spacing ≈2.90 Å of β-Sn (calibrated from the 3.26 Å Ge spacing). Most particles are oriented so that $(111)_{Ge}$ is approximately parallel to $(200)_{\beta\text{-}Sn}$. The thick Moire fringes associated with β-Sn result from the nearly parallel reflecting planes of 111_{Ge} and $200_{\beta\text{-}Sn}$. The double diffracted reflections are shown in the FFT.

In addition to the fine β-Sn particles, we observe another form of Sn particles within a grain. Fig. 2 is the HRTEM image of one such particle, shown in Fig. 1(b), close to the [011] zone of Ge, displaying reflections corresponding to spacing of ≈3.75 Å, which is the lattice spacing of 111 of α-Sn, (see the FFT and inverse fast-Fourier transform (IFFT) image in the left and right inset, respectively). The double diffracted spots are also indicated in the FFT. The FFT was calibrated with respect to the lattice spacing of 111 Ge spots (shown in Fig. 2 as well). The FFT was determined from several particles, and in every case, we obtain strong 111 α-Sn reflections close to the [011] Ge zone.

Fig. (3) shows a DSC trace during heating with a strong endothermic peak in the range of 225 to 230°C that can be attributed to melting of the Sn particles. In addition to

the strong endothermic peak due to melting, a broad but distinct endothermic peak appears much earlier at a peak temperature of 100°C. This small peak does not persist in the subsequent heating runs, suggesting that it is a result of the transformation of metastable nanoparticles of α-Sn to β-Sn. The subsequent cooling curve shows, Fig. 3, that some Sn particles undercool to a very great extent with a solidification peak temperature of 160°C.

The proposed pathways for the formation of Sn nanodots are shown schematically in Fig.4. The free energy vs. composition curve for the Ge-Sn solid solution below the eutectic temperature shows the existence of a driving force (ΔG_1) for the formation of metastable α-Sn in Ge matrix. The free energy of Ge-rich and Sn-rich portions lies on the same free energy curve as the crystal structures of Ge and α-Sn are the same. Another pathway for the formation of Sn particles is through solidification of Sn rich liquid droplets. The solidification of the Sn rich liquid will always result in near-pure β-Sn and Ge with a driving force of (ΔG_3) as shown in Fig. 4. Note that there is no driving force available for α-Sn in this route. Thus, the necessary condition to form α-Sn in the Ge matrix is through the decomposition of a supersaturated solid solution of Ge(Sn). The equilibrium solubility of Sn in Ge can be increased by non-equilibrium processing methods, such as MBE [15] and rapid solidification.

The possible mechanism of stabilization of low-temperature allotropic tin modification above ambient temperature in the form of extremely fine precipitates embedded in Ge matrix may be due to the lower interfacial energy of Ge/α-Sn interface as compared to the Ge/β-Sn interface, which would act as a barrier to nucleation of β-Sn. The other stabilizing factor would be the higher activation volume of diffusion through the α-Sn/Ge interphase boundaries under the compressive stress [16].

4. Summary and Conclusion:

We have demonstrated that the diamond cubic form of Sn nanoparticles is stabilized above room temperature in a Ge matrix produced using rapid solidification of Ge-6.3at% Sn. The diamond cubic Sn forms by the decomposition of a Ge-Sn solid solution, which gives the thermodynamic driving force necessary for the formation of semiconducting α-Sn.

Acknowledgments:

Funding for this project was provided by ONR through the Naval Research Laboratory's 6.1 Research Program.

References:

1. S. Groves, W. Paul, Phys. Rev. Lett., 11 (1963) 194.
2. R.V. S. Jensen, T. G. Pedersen, K. Pedersen, Phys. Stat. Solidi C 8 (2011) 1002

3. P. Moontragoon, N. Vukmirovic, Z. Ikonic, P. Harrison, J Appl Phys. 103, (2008) 103712
4. S. Kufner, J. Furthmuller, L. Matthes, F. Bechstedt, Nanotechnology, 24 (2013) 9.
5. Y. Lei, P. Mock, T. Topuria T, N. D. Browning, R. Ragan, K. S. Min and H. A. Atwater, Appl Phys Lett. 82 (2003) 4262.
6. I. Arslan, T.J.V. Yates, N.D. Browning, P. A. Midgley, Science, 309 (2005) 2195.
7. H.S. Im, Y. J. Cho, Y. R. Lim, C. S. Jung, D. M. Jang, J. Park, F. Shojaei and H. S. Kang, ACS Nano, 7 (2013) 11103
8. R. F. C. Farrow, D. S. Robertson, G. M. Williams, A. G. Cullis, G. R. Jones, I. M. Young and P.N. J. Dennis, J Cryst. Growth., 54 (1981) 507.
9. D. Kondo, K. Sakamoto, M. Shima, W. Takeyama, K. Nakamura, K. Ono, Y. Kasukabe and M. Oshima, Phys. Rev. B., 70 (2004) 233314
10. M. Bauer, J. Taraci, J. Tolle, A. V. G. Chizmeshya, S. Zollner, D. J. Smith, J. Menendez, C. Hu and J. Kouvetakis, Appl. Phys Lett. 81 (2002) 2992.
11. S. Takeuchi, Y. Shimura, O. Nakatsuka, S. Zaima, M. Ogawa, A. Sakai, Appl Phys Lett., 92 (2008) 231916.
12. V.G. Deibuk and Y.G. Korolyuk, Physics and Techniques of Semiconductors, 36 (2002) 1153
13. W.T. Kim and B. Cantor, J. Mater. Sci. 26 (1991) 2868
14. L. Li, B. Yang, B. Zhao, A. S. Abyzov, J. W. P. Schmelzer, C Schick, F. Lu, Q. Zhai and Y. Gao, Materials Research Express, 1 (2014) 045012
15. S. Biswas, J. Doherty, D. Saladukha, Q. Ramasse, D. Majumdar, M. Upmanyu, A. Singha, T. Ochalski, M. A. Morris and J. D. Holmes, Nature comm., 7 (2016) 11405
16. B. B. Straumal, L. M. Klinger and L. S. Shvindlerman, Scripta Metall. 17 (1983) 275

Figure Captions

Fig. 1. a) A TEM image of a coarse β-Sn particle at the triple point. b) A bright-field TEM image showing a nanodispersion of Sn particles in the Ge matrix. C) HRTEM showing β-Sn in the Ge matrix. d) FFT from the particle and part of the matrix.

Fig. 2. HRTEM image showing an α-Sn particle in the Ge matrix. The FFT is given as a left inset, showing 111 α-Sn reflections. The IFFT image constructed from 111 α-Sn reflections is shown as a right inset.

Fig. 3. DSC output as a function of temperature. Inset shows the magnified view of the endotherm around 100°C.

Fig.4. Schematic diagram of Gibbs free energy as function of composition showing the existence of a driving force for the formation of α-Sn in Ge.

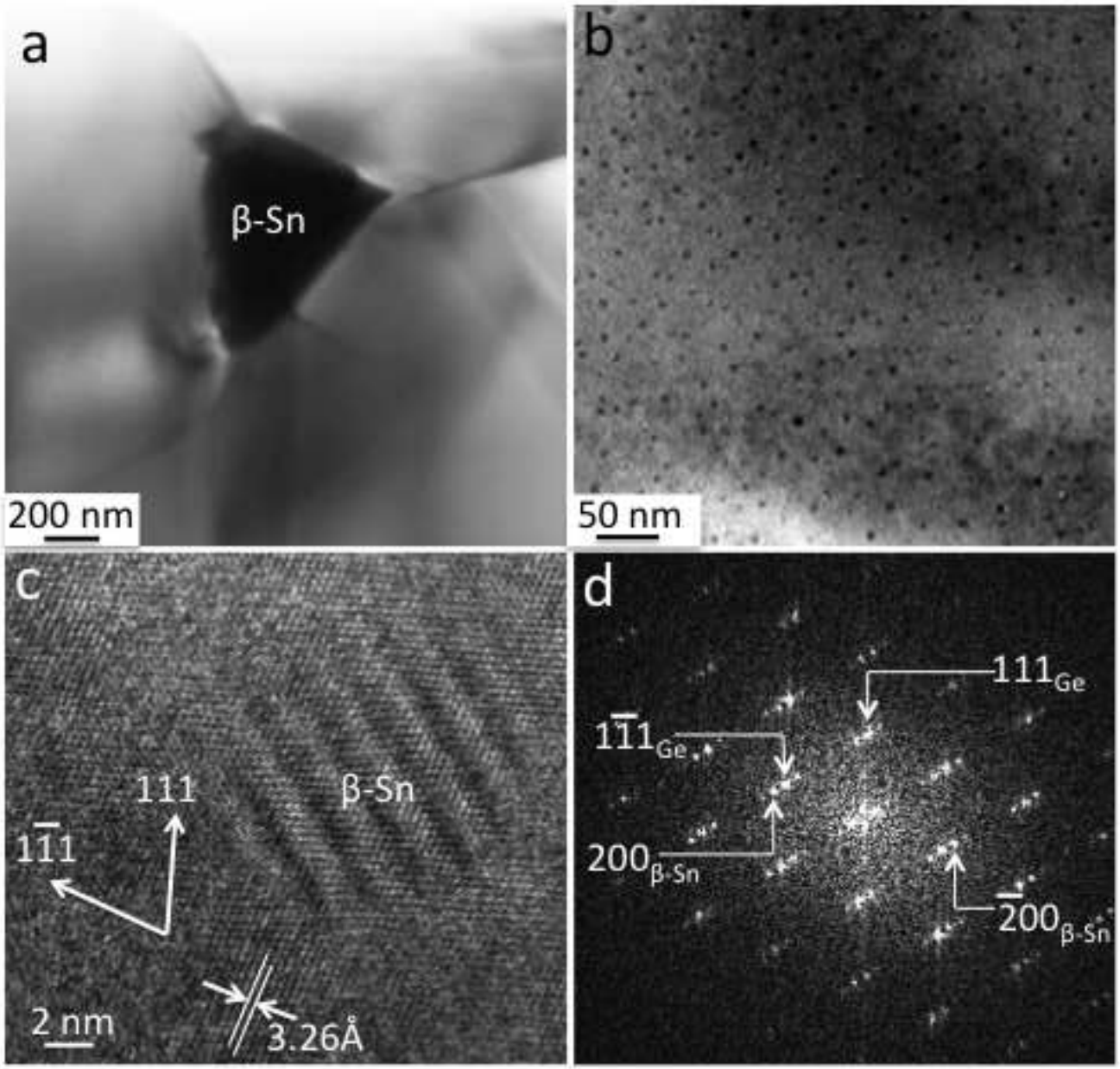
a
β-Sn
200 nm
b
50 nm
c
111
$1\bar{1}1$
β-Sn
2 nm
3.26Å
d
111_{Ge}
$1\bar{1}1_{Ge}$
$200_{\beta\text{-}Sn}$
$\bar{2}00_{\beta\text{-}Sn}$

Fig. 1

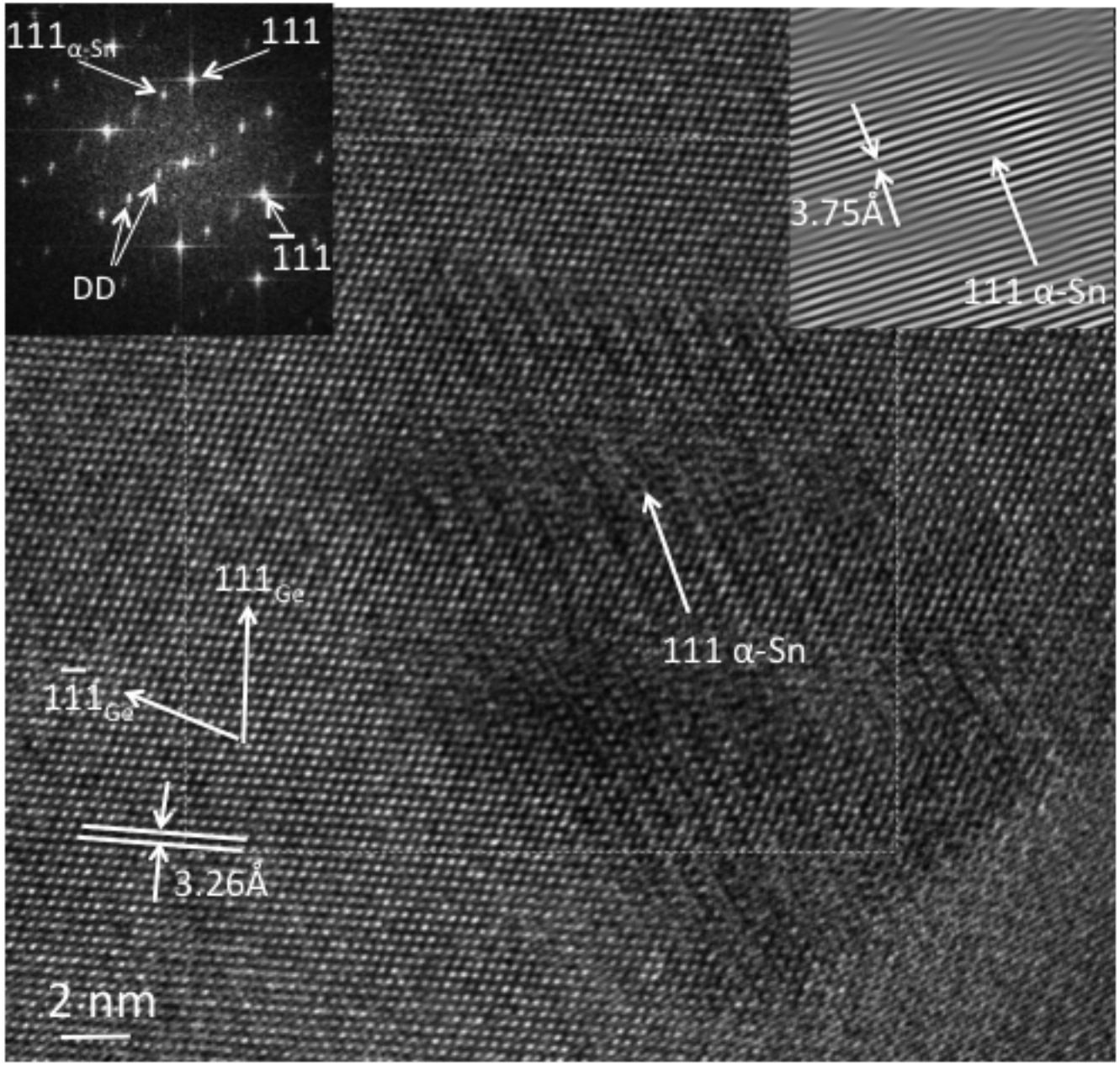

Fig. 2

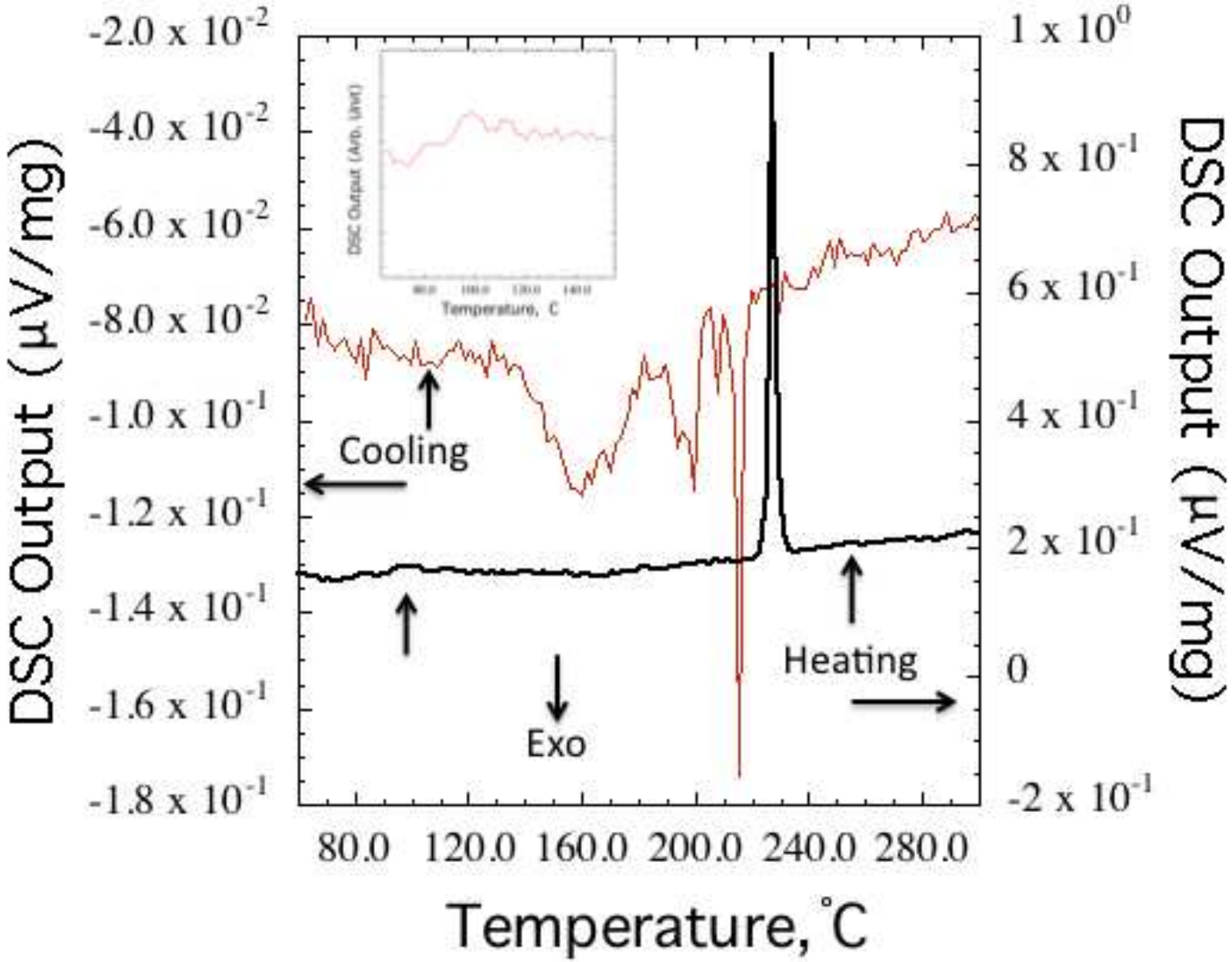
DSC Output (μV/mg)
-2.0 x 10-2
-4.0 x 10-2
-6.0 x 10-2
-8.0 x 10-2
-1.0 x 10-1
-1.2 x 10-1
-1.4 x 10-1
-1.6 x 10-1
-1.8 x 10-1
1 x 100
8 x 10-1
6 x 10-1
4 x 10-1
2 x 10-1
0
-2 x 10-1
DSC Output (μV/mg)
80.0 120.0 160.0 200.0 240.0 280.0
Temperature, ˚C
Cooling
Exo
Heating
DSC Output (Arb. Unit)
Temperature, C

Fig. 3

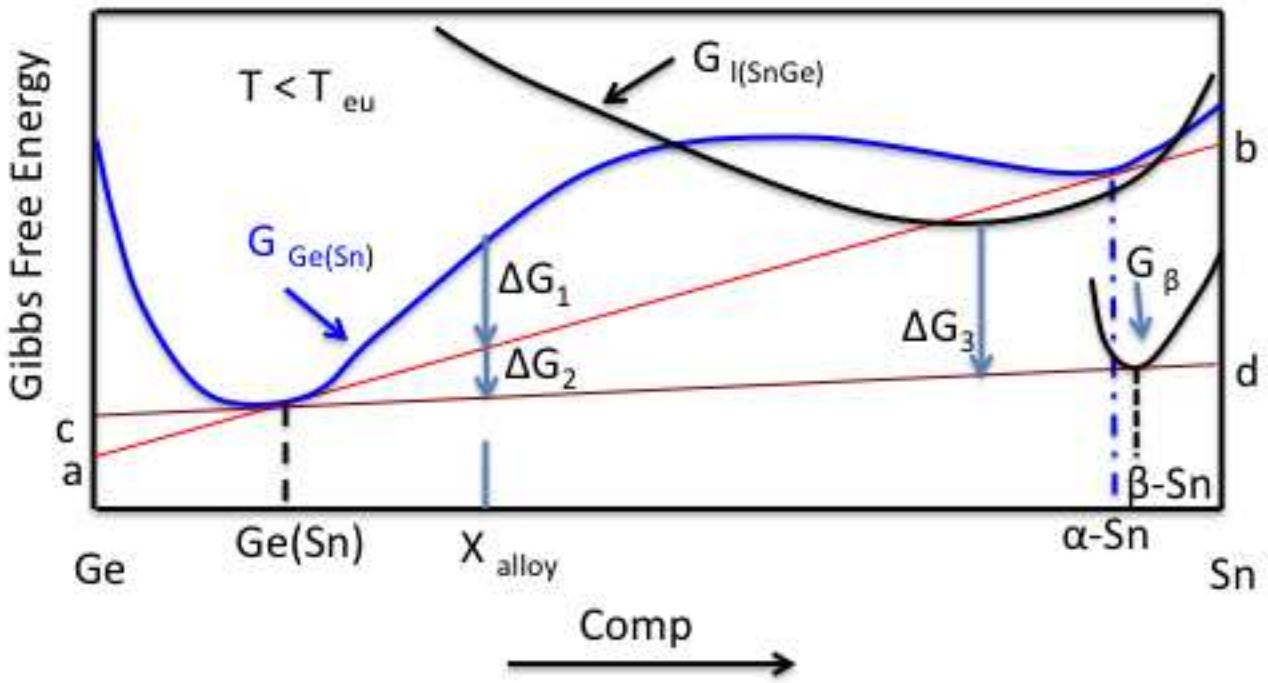
Gibbs Free Energy
T < T eu
G l(SnGe)
G Ge(Sn)
ΔG1
ΔG2
ΔG3
G β
b
d
c
a
β-Sn
Ge
Ge(Sn)
X alloy
α-Sn
Sn
Comp

Fig. 4